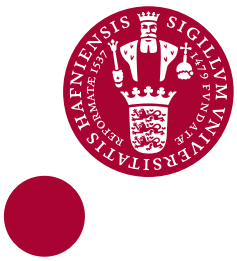

Sea Surface Temperature Variability on the SEGreenland Shelf (1796–2013 CE) and Its Influence on Thrym Glacier in Nørre Skjoldungesund

Wangner, David Johannes; Sicre, Marie-Alexandrine; Kjeldsen, Kristian; Jaeger, John M.; Bjørk, Anders Anker; Vermassen, Flor; Sha, Longbin; Kjær, Kurt H.; Klein, Vincent; Andresen, Camilla S.

Published in:
Paleoceanography and Paleoclimatology

DOI:
10.1029/2019PA003692

Publication date:
2020

Document version
Publisher's PDF, also known as Version of record

Paleoceanography and Paleoclimatology

RESEARCH ARTICLE
10.1029/2019PA003692

Sea Surface Temperature Variability on the SE-Greenland Shelf (1796–2013 CE) and Its Influence on Thrym Glacier in Nørre Skjoldungesund

David J. Wangner[1,2], Marie-Alexandrine Sicre[3], Kristian K. Kjeldsen[1], John M. Jaeger[4], Anders A. Bjørk[5], Flor Vermassen[1,2], Longbin Sha[6], Kurt H. Kjær[2], Vincent Klein[3], and Camilla S. Andresen[1]

[1]Department of Glaciology and Climate, Geological Survey of Denmark and Greenland (GEUS), Copenhagen, Denmark, [2]Centre for GeoGenetics, GLOBE Institute, University of Copenhagen, Copenhagen, Denmark, [3]Sorbonne Université, Campus Pierre et Marie Curie, LOCEAN, Paris, France, [4]Department of Geological Sciences, University of Florida, Gainesville, FL, USA, [5]Department of Geosciences and Natural Resource Management, University of Copenhagen, Copenhagen, Denmark, [6]Department of Geography and Spatial Information Technology, Ningbo University, Ningbo, China

Abstract Heat transport via ocean currents can affect the melting of marine-terminating glaciers in Greenland. Studying past changes of marine-terminating glaciers allows assessing the regional sensitivity of the Greenland Ice Sheet to ocean temperature changes in the context of a warming ocean. Here, we present a high-resolution multiproxy marine sediment core study from Skjoldungen Fjord, close to the marine-terminating Thrym Glacier. Grain-size data are obtained to reconstruct the calving activity of Thrym Glacier; sortable silt is used as a proxy for fjord water circulation, and sea surface temperatures (SSTs) are reconstructed from alkenone paleothermometry (Uk'37). Measurements of ^{210}Pb, ^{137}Cs, and ^{14}C indicate that the core covers the past 220 years (1796–2013 CE). Comparisons with modeled SST data (Hadley Centre Sea Ice and SST) and instrumental temperatures (International Council for the Exploration of the Sea) suggest that the SST proxy record reflects temperature variability of the surface waters over the shelf and that alkenones are advected into the fjord. Additionally, average temperatures and the amplitude of fluctuations are influenced by alkenones advected from upstream the Irminger Current. We find that the SST record compares well with other alkenone-based reconstructions from SE-Greenland and thus features regional shelf water variability. The calving activity as well as the terminus position of Thrym Glacier did not seem to respond to the SST variability. Limited ice-ocean interactions owing to the specific setting of the glacier would explain this. Instead, the fjord circulation may have been influenced by enhanced meltwater production as well as to larger scale changes in the Atlantic Meridional Overturning Circulation.

Key Points:
- Alkenone-based sea surface temperature reconstructions reveal common SE-Greenland shelf variability during the 20th century
- Increasing ocean temperature did not result in a retreat of Thrym Glacier
- Sortable silt parameters indicate that fjord water column flow is influenced by increased meltwater release and/or shelf water circulation

Supporting Information:
- Supporting Information S1
- Data Set S1

Correspondence to:
D. J. Wangner,
dawangner@gmail.com

Citation:
Wangner, D. J., Sicre, M.-A., Kjeldsen, K. K., Jaeger, J. M., Bjørk, A. A., Vermassen, F., et al. (2020). Sea surface temperature variability on the SE-Greenland shelf (1796–2013 CE) and its influence on Thrym Glacier in Nørre Skjoldungesund. *Paleoceanography and Paleoclimatology*, *35*, e2019PA003692. https://doi.org/10.1029/2019PA003692

Received 10 JUN 2019
Accepted 14 NOV 2019
Accepted article online 5 DEC 2019

1. Introduction

Observations during the 20th and 21st centuries show that most glaciers in SE-Greenland underwent large fluctuations in the position of their termini. The coincidence between two distinct periods of climate warming and high retreat rates, one in the 1930s and a second in the early 2000s, suggest a common climate forcing (Bjørk et al., 2012; Khan et al., 2015; Straneo et al., 2012). Murray et al. (2010) proposed oceanic forcing as a common driver for the early 2000s glacier speedup and thinning in SE-Greenland. Although multiple studies have demonstrated a link between increasing ocean temperatures and the retreat of marine terminating glaciers, the physical mechanisms involved in glacier mass loss are still unclear (Straneo & Heimbach, 2013). Despite the general common trend in termini fluctuations, historic observations reveal that individual glaciers can show umpteen responses to similar climatic forcing (Bjørk et al., 2012; Khan et al., 2015; Motyka et al., 2017; Straneo et al., 2012).

Improving predictions of the behavior of marine-terminating glaciers in a future warmer climate requires a better understanding of the processes involved in ocean-forced glacier melt. This can be accomplished via studies targeting past and present changes; however, instrumental observations of ocean temperature variability are scarce, locally restricted, and limited in duration. Fjord sediment cores usually provide high sedimentation rates allowing to extend environmental records beyond the instrumental time period at subdecadal to annual scale (Dowdeswell, 1987). In this study, we provide new ocean data representing the

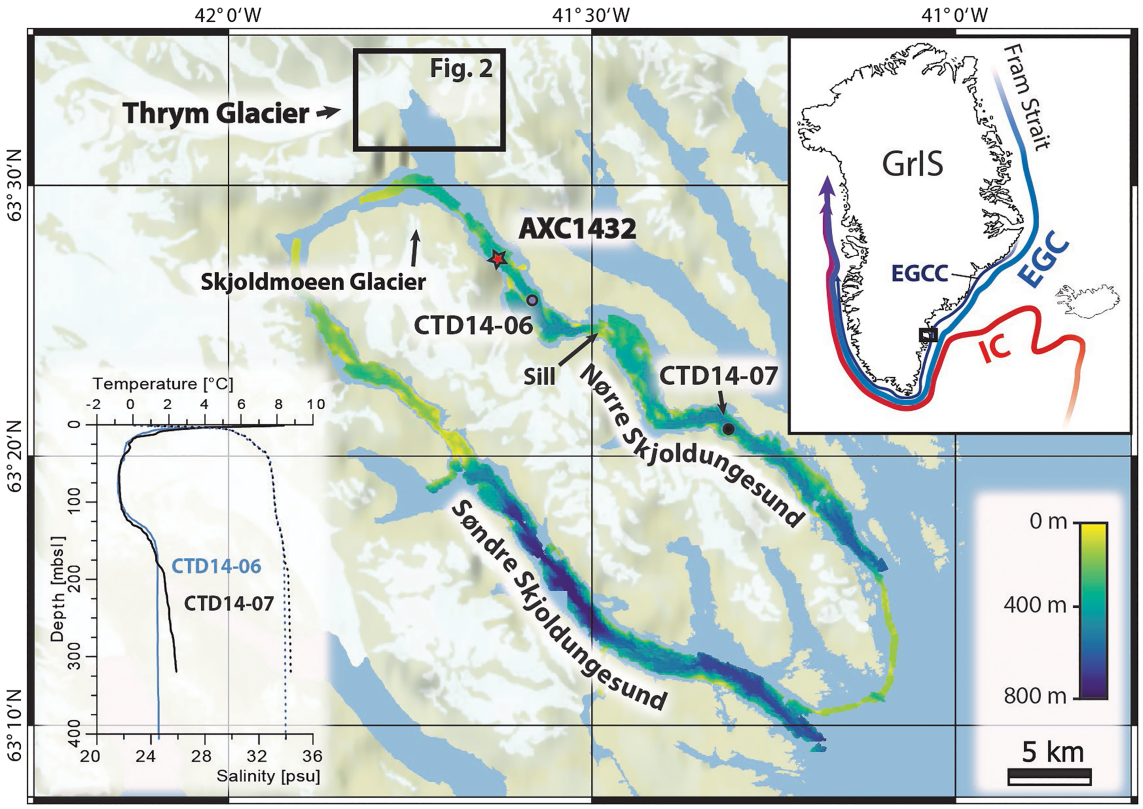

Figure 1. Map of the Skjoldungen area with bathymetry data from Nørre and Søndre Skjoldungesund Fjords (Kjeldsen et al., 2017). The core location is indicated by a red star. Graph inset show CTD measurements (obtained August 2014) from locations CTD14-06 and CTD14-07 (Kjeldsen et al., 2017). Solid lines show temperature profile, while dotted lines show salinity profiles. The inset map of Greenland indicates the major oceanographic currents around southern Greenland: Irminger Current (IC), East Greenland Current (EGC), and East Greenland coastal Current; the black box represents the location of the Skjoldungen area.

past 220 years in high detail (down to 1- to 2-year sampling resolution) using a marine sediment core from Skjoldungen Fjord in SE-Greenland (Figure 1). The proxy ocean data are compared with the available instrumental oceanographic temperature observations and other proxy temperature records from offshore SE-Greenland.

Sediment cores have additionally been used to investigate the link between ocean warming and glacier dynamics of some of the largest marine-terminating glaciers in Greenland, such as Jakobshavn Isbræ (Holland et al., 2008; Lloyd, 2006, 2011; Andresen et al., 2011, Wangner et al., 2018), Helheim Glacier (Andresen et al., 2012, 2013, 2017), and Kangerlussuaq glacier (Vermassen, Bjørk, et al., 2019). While the glacier geometry of these glaciers are characterized by deep subglacial troughs connected directly to the fjords, smaller glaciers terminating in shallower fjords such as Thrym Glacier, which terminates into Skjoldungen Fjord, usually have a limited ice-ocean interface. However, the combined melt from all of Greenland's numerous smaller glaciers has the potential to contribute significantly to future sea-level rise and affect regional oceanography by adding freshwater and changing the surface water buoyancy (Barrier et al., 2014). It is thus similarly important to study glaciers with different geometrical settings. Here, we reconstruct the calving behavior of Thrym Glacier back in time by measuring the amount of ice-rafted debris (IRD) in the sediment core from Skjoldungen Fjord. Furthermore, the mean grain size of the sortable silt ($\overline{SS}$) was measured in order to investigate changes in the fjord water circulation. By comparing the reconstructed 220-year long record of alkenone-based sea surface temperature (alkSST), plume dynamics, iceberg production, and observed terminus position of Thrym Glacier, we explore the links between these environmental changes.

2. Study Area

The Skjoldungen Island located in SE-Greenland is surrounded by the Skjoldungen Fjord systems with two main branches: the southern fjord (Søndre Skjoldungesund) and the northern fjord (Figure 1). Towards the

Figure 2. Landsat Satellite image of Thrym Glacier (June 2014) with observed terminus positions since 1933.

northwest, the two fjords are connected by a shallower section with water depths not exceeding 70 m. At the head of Nørre Skjoldungesund, the marine-terminating Thrym Glacier calves icebergs into the fjord, while the remaining local glaciers and icecaps surrounding the fjord are land terminating, with a few extending to sea level during the Little Ice Age (LIA) (e.g., Skjoldmøen Glacier, Figure 1; Bjørk et al., 2012). The distance between the Thrym Glacier terminus and the open shelf area is around 50 km. The water depth of Nørre Skjoldungesund increases gradually from 340 m near Thrym Glacier to 590 m at the fjord entrance and is intervened by a ~210-m depth sill located ~20 km from Thrym Glacier (Kjeldsen et al., 2017).

The 1.6-km wide terminus of Thrym Glacier has been relatively stable over the past 80 years, (Figure 2) with minor fluctuations in a range of about 300 m as evident from the LIA trimline mapping and historical aerial photographs and satellite imagery from 1933 onwards (Bjørk et al., 2012; Kjeldsen et al., 2015).

The ocean temperature on the SE-Greenland shelf is mainly the result of the interaction between two major regional currents: The Irminger Current (IC), a bifurcation of the Gulf Stream carrying warm salty waters and the overlaying East Greenland Current (EGC), forms a relatively cold and freshwater layer above down to a depth of 150 to 200 m (Sutherland et al., 2013; Sutherland & Pickart, 2008). Additionally, the East Greenland coastal Current is formed by meltwater derived from the Greenland Ice Sheet forming a freshwater surface current along the west coast of Greenland. These three currents meet along the shelf of SE-Greenland and mix gradually on their way around the southern tip of Greenland but can still be distinguished as far north as Disko Bugt in West Greenland (Myers et al., 2007). The interaction between the IC and EGC is largely controlled by the dynamics of the Subpolar Gyre (SPG) and changes of the sea ice outflow from the Arctic Ocean (Häkkinen & Rhines, 2004; Hátún et al., 2005). Moreover, surface water properties off SE-Greenland are also influenced by seasonal to daily variations of the freshwater input from the Greenland Ice Sheet through meltwater runoff and iceberg melting (Sutherland & Pickart, 2008). The IC, EGC, and surface meltwater are also present in Nørre Skjoldungesund; CTD measurements from July 2014 (Figure 1, Kjeldsen et al., 2017) document a thin meltwater layer in the upper approximately 20 m. Temperatures range between 8°C in the top and 0°C in the lower part of the layer along with a low salinity of 29 of psu. The water mass positioned between 20- and 120-m depths is characterized by low temperatures between −1°C and 0°C and a salinity of 33 indicative of EGC waters. Below 150-m depth, the temperature increases to 1–2°C, and salinity remains constant at 34, which indicates a stronger influence of IC water masses within the fjord.

The Hadley Centre Sea Ice and Sea Surface Temperature data set (HadISST) provides observation based but modeled global SST data since 1871 with a grid cell size of about 50 km × 111 km for the northern Atlantic, (Rayner et al., 2003). These data provide an average late summer SST value (for the period 1993–2012) of 5°C just outside Nørre Skjoldungesund, rising to 12°C going 500 km to the East. Combined temperature profiles from outside Nørre Skjoldungesund, obtained from the International Council for the Exploration of the Sea (ICES), show an average temperature of 6.9°C for the uppermost 50 m for the same time period.

3. Methods

The 143-cm long core AXC1432 was recovered in 2014 on board of the wooden schooner *SS ACTIV* in Nørre Skjoldungesund using a Rumohr coring device (Meischner & Rumohr, 1974). The core location lies approximately 13 km from the Thrym Glacier calving front (63.457°N/41.6257°W) in a water depth of 357 m. To provide an optical line scan and to identify potential turbidites, the core was scanned using an Itrax Core scanner at the Natural History Museum of Denmark, Copenhagen. A composite X-ray image was obtained from five digitally merged photographs produced with an YXLON smart 160E/0.4 system at the National Museum of Denmark, Copenhagen (120 s, 3 mA, 90 KV).

3.1. Alkenone Paleothermometry

Alkenone paleothermometry is used to generate a high-resolution record of SST. Alkenone-based temperature reconstructions in the Nordic seas are sparse and often challenged by temperatures below a correlation limit of −5°C (Bendle et al., 2005; Conte et al., 2006; Filippova et al., 2016; Sicre et al., 2002). Previous studies have shown that the local signal in SE-Greenland fjords can be biased by nearby highly alkenone productive waters such as south of Iceland or local upwelling, calling for cautious interpretation of the alkSST reconstruction (Andresen et al., 2013, 2017). The bias that can be introduced by surface current advection in regions with a weak local production has also been demonstrated (Conte et al., 2003; Rühlemann & Butzin, 2006). This requires that the geographical source region of the alkenones deposited in Nørre Skjoldungesund sediments is assessed and taken into account.

Samples were analyzed for alkenones at LOCEAN (Paris) in a 1-cm resolution at a Varian 3400CX gas chromatograph equipped with a CPSil5 capillary column (50 m length, 0.32 i.d., and 0.25-mm film thickness), a Flame ionization detector and a septum programmable injector. Helium was used as a carrier gas. Lipids were previously extracted from freeze-dried samples (of 2.4–6.5 g of dry sediment) using a dichloromethane/methanol mixture (2:1 v/v). Fractionation was then performed by silica gel chromatography adapted from Ternois et al. (1997). C_{37} alkenones measured in the samples include $C_{37:2}$, $C_{37:3}$, and $C_{37:4}$. Due to low concentrations of alkenones, the unsaturated index ($U^{K'}_{37}$) could be calculated for 113 samples out of 143. We used the BAYSPLINE calibration of Tierney and Tingley (2018) to translate the index into temperature. For comparison, we also used the linear relationship established by Prahl and Wakeham (1987).

$$U^{K'}_{37} = \frac{C_{37:2}}{C_{37:2} + C_{37:3}} = 0.034T + 0.039$$

Internal precision of SST estimates was ±0.6°C. (Prahl et al., 1988)

3.2. Ice-rafted Debris

In order to extend information on the calving behavior of Thrym Glacier back in time, the percentage of sand within the sediment core was measured. This parameter represents the amount of IRD, which is commonly used as an indicator for the iceberg rafting from marine-terminating glaciers (Andresen et al., 2012, 2017; Andrews et al., 1997; Andrews, 2000; Dowdeswell, 1987; Dyke et al., 2017; Syvitski & Shaw, 1995; Vermassen, Wangner, et al., 2019; Wangner et al., 2018). These studies indicate that iceberg rafting in fjords not only depends on the iceberg production but can also be modulated by a variety of processes including glacier margin type (shelf versus calving glacier), changes to transit time of icebergs down the fjord or changes to the distance between coring site and glacier margin.

Grain-size analyses were undertaken continuously at a 1-cm sampling resolution, by wet sieving through 63- and 150-μm *Retsche* sieves with a sample size between 2.9 and 6.8 g of dry sediment. The upper 2 cm of the core did not provide enough sampling material and thus could not be measured. Grains heavier than 0.1 g were manually excluded from the >150 μm of fraction to avoid disproportional impact of single grains (Wangner et al., 2018).

3.3. Sortable Silt

The water circulation within fjords is a major unknown in understanding ice-ocean interactions (Motyka et al., 2003; Straneo et al., 2011, 2013). However, it plays a crucial role in heat exchange between the ocean currents, the atmosphere and the glacier (Murray et al., 2010). The mean grain size of SS ($\overline{SS}$) is commonly

used as a proxy for current strength near the sea bed (Bianchi & McCave, 1999; McCave et al., 1995, 2017) and has also been used as a proxy for water renewal rate in Sermilik Fjord (Andresen, Schmidt, et al., 2014). We use the SS^{-} as an indicator to investigate changes in the fjord water circulation in Nørre Skjoldungesund, which can be affected by enhanced meltwater discharge from Thrym Glacier or by external shelf currents. McCave and Andrews (2019) demonstrate that sortable silt data from laser particle-size analyzers is valid in glacimarine settings, so the <63 μm of fraction was analyzed continuously at a 1-cm sampling resolution between 3 and 143 cm, using a *Malvern Mastersizer 3000*. Between 65 and 90 mg of the samples were homogenized in an agate mortar and put in a test tube. Samples were then dispensed with 15-ml 0.005 M tetra-sodium-diphosphate-decahydrate and treated with an ultrasound probe for 45 s.

Since the grain-size composition at our core site is affected by the vicinity of a marine terminating glacier, sortable silt values can be biased by potential input from ice rafting and may obscure a signal from current sorting (McCave & Andrews, 2019). To determine the valid application of SS^{-} to our sediment record, we followed the data processes procedure applied in McCave and Andrews (2019), who test for an IRD influence by calculating the correlation between sortable silt percentage within the <63 μm fraction (SS%) and SS^{-} (Figure S1, supplementary information). Low correlation implies high IRD contribution. Our resulting correlation of $R = 0.87$ lies above their proposed minimum correlation coefficient of 0.5 for a primarily current-influenced sortable silt record.

3.4. Chronology

A chronology was developed using ^{210}Pb excess ($^{210}Pb_{xs}$; $T_{1/2} = 22.3$ years),^{137}Cs ($T_{1/2} = 30$ years), and one ^{14}C sample. Seven sediment samples, from the top 50 cm of the core, were freeze-dried, powdered, and measured for radioisotopes on a low-background, well-type germanium detector at the Department of Geological Sciences, University of Florida, USA. Activities of ^{210}Pb, ^{226}Ra, and ^{137}Cs were corrected for self-adsorption and decay since core collection. The ^{14}C date was obtained from an unidentified carbonate shell fragment, found at 115 cm (measured at the University of Lund).

3.5. Statistical Analysis

In order to evaluate the statistical significance of correlations between the data, comparisons with synthetic red-noise time series was used (Knudsen et al., 2014). The synthetic data were modeled as an AR1 process following the procedure of Schulz and Mudelsee (2002) with characteristic memory factors (f) equal to that obtained for the raw SST data. The characteristic memory factor (f) was obtained using the covariance function for the AR1 process given as $\mathrm{cov}(X(t_i), X(t_j)) = F_0 \times f^{|j-i|}$, where F_0 is the variance and $\mathrm{cov}(X(t_i), X(t_j))$ is the covariance observed at$|j - i|$time steps from zero lag. A total of 10,000 synthetic SST data sets were simulated using a Monte Carlo approach, and the correlation coefficients obtained between the synthetic SST data and other alkSST records, as well as the HadISST data, were compared to those obtained for the actual SST data.

4. Results

The sediment in core AXC1432 consists of a massive clay and silt-rich diamicton indicating iceberg rafting. X-radiograph images and the optical scan of the sediment (Figures 3a and 3b) reveal a sedimentary structure between 82 and 84 cm, which is interpreted as a turbidite and thus excluded from data interpretation.

4.1. Alkenones

The alkSST values after both calibrations range between 5°C and 12°C (Figure 3e). The calibration according to Prahl and Wakeham (1987) results in 0.4–0.44°C higher temperatures (mean = 7.65°C), than the calibration based on BAYSPLINE (mean = 7.23°C, Tierney & Tingley, 2018). In the following, only the results from the BAYSPLINE calibration are discussed.

From the bottom of the core at 143 cm until 70 cm depth, temperatures vary between 6.5°C and 9.2°C, while above 70 cm, the amplitude of the variations increases to 4.5–11.6°C with maximum values found at 60 cm (10.7°C) and 46 cm (11.6°C) followed by a decline between 41 and 30 cm (to 6–7°C). Above 30 cm, temperature increases again with three maxima centered at 25, 15, and 9 cm. The lowest value of 4.5°C was found at 6 cm.

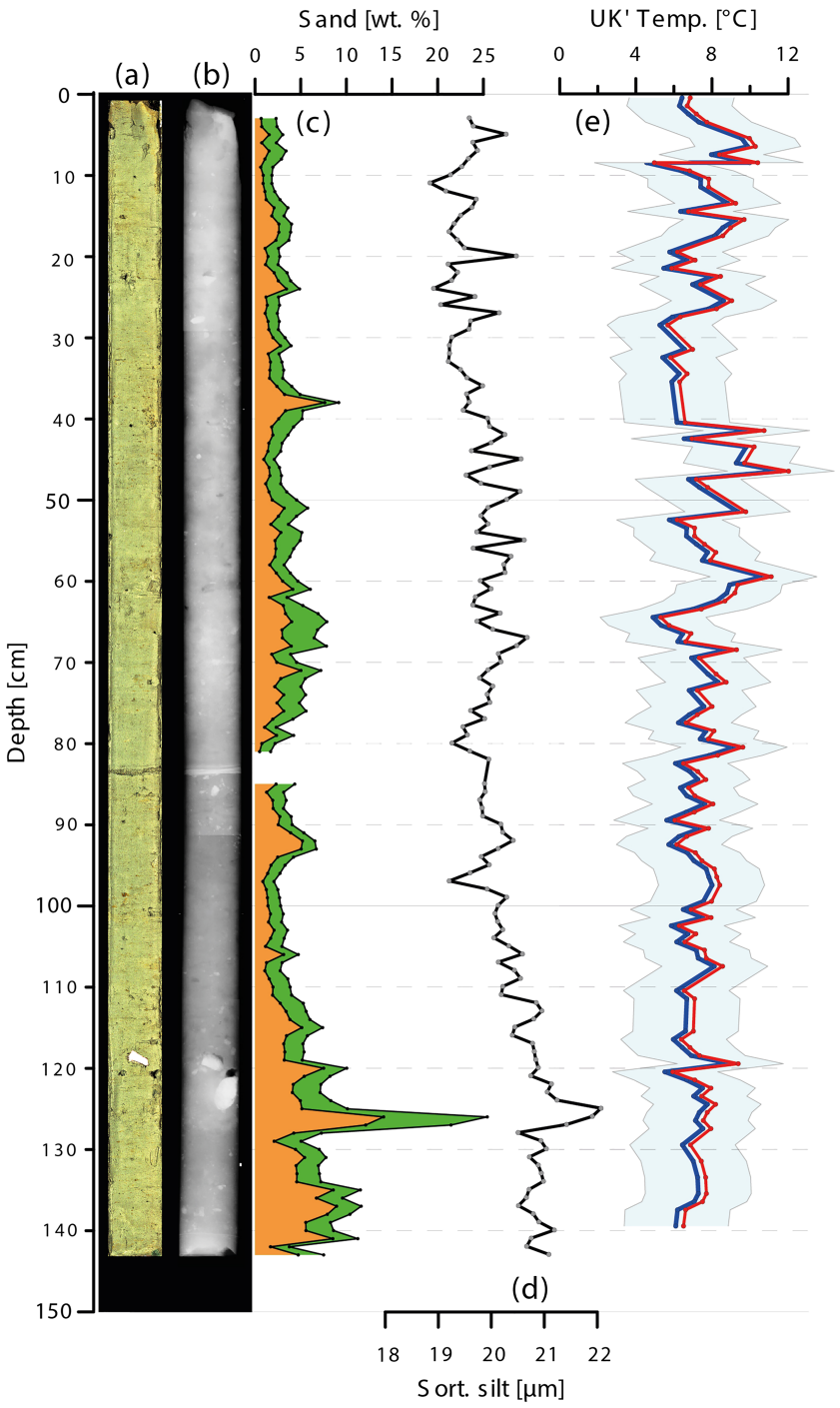

Figure 3. Data from core AXC1432 versus depth: (a) optical scan of the core with adjusted contrast and brightness, (b) merged X-radiograph image, (c) grain-size analyses with the 63–150 μm sand fraction (green shading) cumulative to the 150–2,000 μm sand fraction (orange shading), (d) mean sortable silt diameter, and (e) temperature reconstruction based on the $U^{K'}_{37}$ index. BAYSPLINE calibration in blue (Tierney & Tingley, 2018) with sigma 1 error in light blue. Red line shows the calibration according to (Prahl & Wakeham, 1987). Light grey horizontal lines are inserted for visual aid.

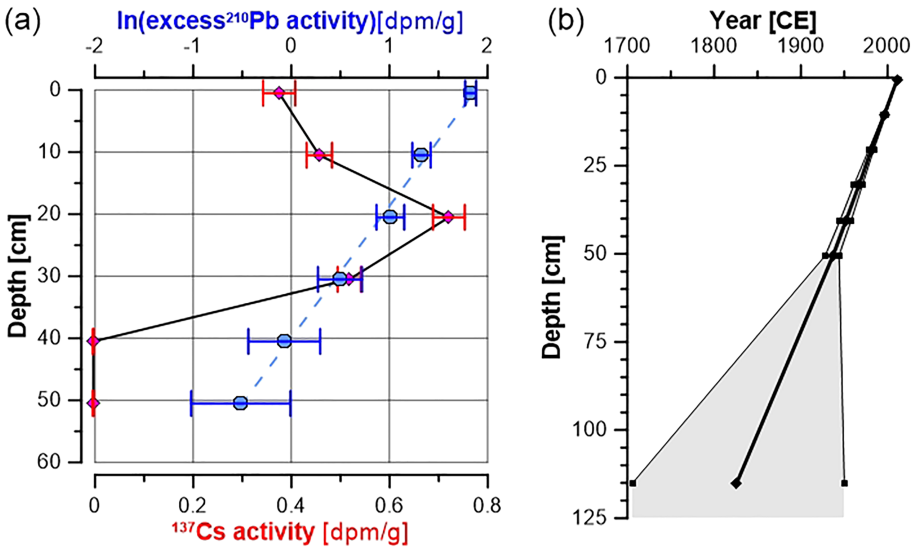

Figure 4. (a) Downcore profile of activity in excess ^{210}Pb (blue) shown on a logarithmic scale versus depth. ^{137}Cs activity is in red. (b) Results of dating versus depth, with the oldest/youngest calibrated ages in thin line and the average indicated by the thick line.

4.2. Ice-rafted Debris

The 150–2,000 μm fraction varies between 0.5 and 9 weight% (wt. %), whereas the 63–150 μm fraction shows values between 1 and 4 wt.% (Figure 3c). Between 126 and 127 cm exceptionally high values are observed in the 63–150 μm fraction (11.3 wt.%) and in the >150 μm fraction (14.1 wt.%). Although the grain size varies, a general decrease in the sand content is observed from the bottom of the core at 143 cm towards the top with specifically higher content of coarser grains from 143 to 120 cm. Using X-ray images of the core (Figure 3b) two centimeter-sized clasts are observed around 122 cm. Above 120 cm, the grain size exhibits lower variability mostly between 0.5 and 5 wt.%, with one peak at 38 cm depth reaching 7.6 wt.%.

4.3. Sortable Silt

In similarity with the sand content, the $\overline{SS}$ values show a decreasing trend from the bottom to the top of the core (Figure 3d). Highest values were measured between 143 and 112 cm with and an average value of 20.9 μm. A major peak in the $\overline{SS}$ record (22.1 μm) is observed at the same level as the peak in sand content at 126 cm. Between 112 and 80 cm, the $\overline{SS}$ decreases gradually to an average of 20.1 μm with lowest values at 97 cm (19.2 μm) and 80 cm (19.3 μm). Data from the turbidite positioned between 84 and 82 cm are excluded. Between 80 and 40 cm, values increase slightly (Ø, 20.0 μm) followed by the records lowest values in the top of the core between 40 and 0 cm with a minimum value (18.8 μm) at 11 cm and average of 19.5 μm. Higher values are reached at 5-, 13-, 20-, and 27-cm depths.

4.4. Chronology

Sediment chronologies were established for the upper 115 cm of the core. The excess ^{210}Pb activity was modeled using the constant flux-constant sedimentation (CFCS) approach, which has been previously used in adjacent eastern Greenland fjords (Andresen, Schmidt, et al., 2014). A nonlinear model fit of the CFCS was applied to the data using the R programming language and the publicly available package "nlstools" (Baty et al., 2015). All data and code can be found in File S1. A nonlinear model is used instead of the standard linear regression on log-transformed data because of the heteroscedasticity in activity uncertainty, which precludes the use of a linear model fit. The $^{210}Pb_{xs}$ activity values show an exponential decrease in activity, and the preservation of primary physical sedimentary structures seen in the X-radiograph (Figure 3b) indicates minimal bioturbation within the upper 70 cm that could influence the activity

profile. Model results include uncertainty propagation from the model fit on the sedimentation rates and the midpoint fit sedimentation rate, 0.7 cm/yr, is used in the age model for proxy core data (Figure 4b). The ^{137}Cs activity profile shows a first appearance between 30–40 cm dated to 1952– 1967 based on the $^{210}Pb_{xs}$ CFCS age model, supporting the model fit while accounting for the one half-life of Cs-137 decay since 1954, which makes assigning its first appearance to 1954 challenging.

The radiocarbon sample at 115 cm yielded a radiocarbon age of 655 ± 40 year BP. Using the Marine13 calibration curve (Reimer et al., 2013) and a ΔR of 158 ± 51, based on the study of Olsson (1980) from outside Nørre Skjoldungesund, we obtained a calibrated age of 1824 CE for this level (2 sigma: 1706–1950 CE). Linear extrapolation based on the ^{210}Pb dating indicates an age of 1826 CE for the layer at 115 cm. Given the uncertainty in the ΔR value, the close agreement between these two estimates suggest minor changes in sedimentation rate over the upper 115 cm of core.

5. Discussion

5.1. Tracing the Geographical Source Region of Alkenones Deposited in Skjoldungen Fjord

CTD measurements close to the core location in Nørre Skjoldungesund measured in late July 2014 display temperatures up to 8°C in the very surface layer and very low salinities reflecting the melt water layer (Figure 1, Kjeldsen et al., 2017). The temperature drops markedly to around 0°C below this layer (~10 m), while salinity increases. Lower salinity usually hampers the growth of oceanic *Emiliania huxleyi* (Paasche, 2002), implying that the amount of alkenones produced in the warmer upper water layer would be limited in Nørre Skjoldungesund. This makes it unlikely that the reconstructed temperature range between 5°C and 12°C represents SSTs within the fjord. Previous studies from Sermilik Fjord located 350 km north of Skjoldungen (Figure 5a) have already shown that alkenones deposited in the fjord originate mostly from inner shelf waters advected into the fjord and thus reflect values and variability of coastal waters outside the Sermilik Fjord (Andresen et al., 2013).

In order to specify the geographical origin of the alkenones accumulated in the fjord sediments, the variability of alkSST record from Skjoldungen was compared to temperature time series extracted from the HadISST database (Figure 5c; Rayner et al., 2003). These time series are derived from five different grid cells located upstream along the paths of IC and EGC (Figure 5a) and cover the period from 1870 to 2017. Average temperatures for July–October were compiled, as summer is the main production season of alkenones at high latitudes (Sicre et al., 2011, 2014). Only the time series obtained from the grid cell located just outside Nørre Skjoldungesund (Figure 5c, red line) shows a statistically significant correlation with the Skjoldungen alkSST record, although the correlation coefficient is low ($R = 0.202$, 92% level of confidence). This suggests that the variability seen in the alkSST record is to some extent determined by the variability in the nearby shelf waters. However, the reanalyzed HadISST data set may not accurately reflect the local variability of this highly dynamic region with strong temperature gradients. This may partly explain the low correlation between the alkSST record from Nørre Skjoldungesund and the proximal HadISST data set and the lack of statistical significant correlation with data from grid cells upstream the IC.

For a better comparison with in situ SST observations, a time series of average September to October SSTs (no summer data available) was produced for the time period from 1993 to 2012. It is based on the upper 50 m of 26 CTD profiles within a narrow spatial area outside of Nørre Skjoldungesund (www.ICES.dk; Figures 5a, 5b, and 5d). The general variability is similar in the instrumental record and the alkSST record, but the amplitude of fluctuations is much larger in the alkSST record. This further supports the idea that the pool of alkenones measured in Nørre Skjoldungesund may be strongly influenced by detrital advected alkenones. Compared to the HadISST data, calculated for the same time period and the same area, the measured CTD temperature average is about 1.7°C higher (6.9°C and 5.2°C, respectively) and thus closer to the reconstructed alkSST average of 7.5°C. However, the still 0.6°C higher temperature average in the alkSST record is indicative of a significant contribution of alkenones produced in warmer waters from upstream the IC. Similarly, for the period spanning from 1870 to 2012, the alkSST mean value (7.4°C) is 2.8°C higher than that calculated from HadISST record (4.6°C). Thus, alkSSTs are generally higher than both the CTD and HadISST data.

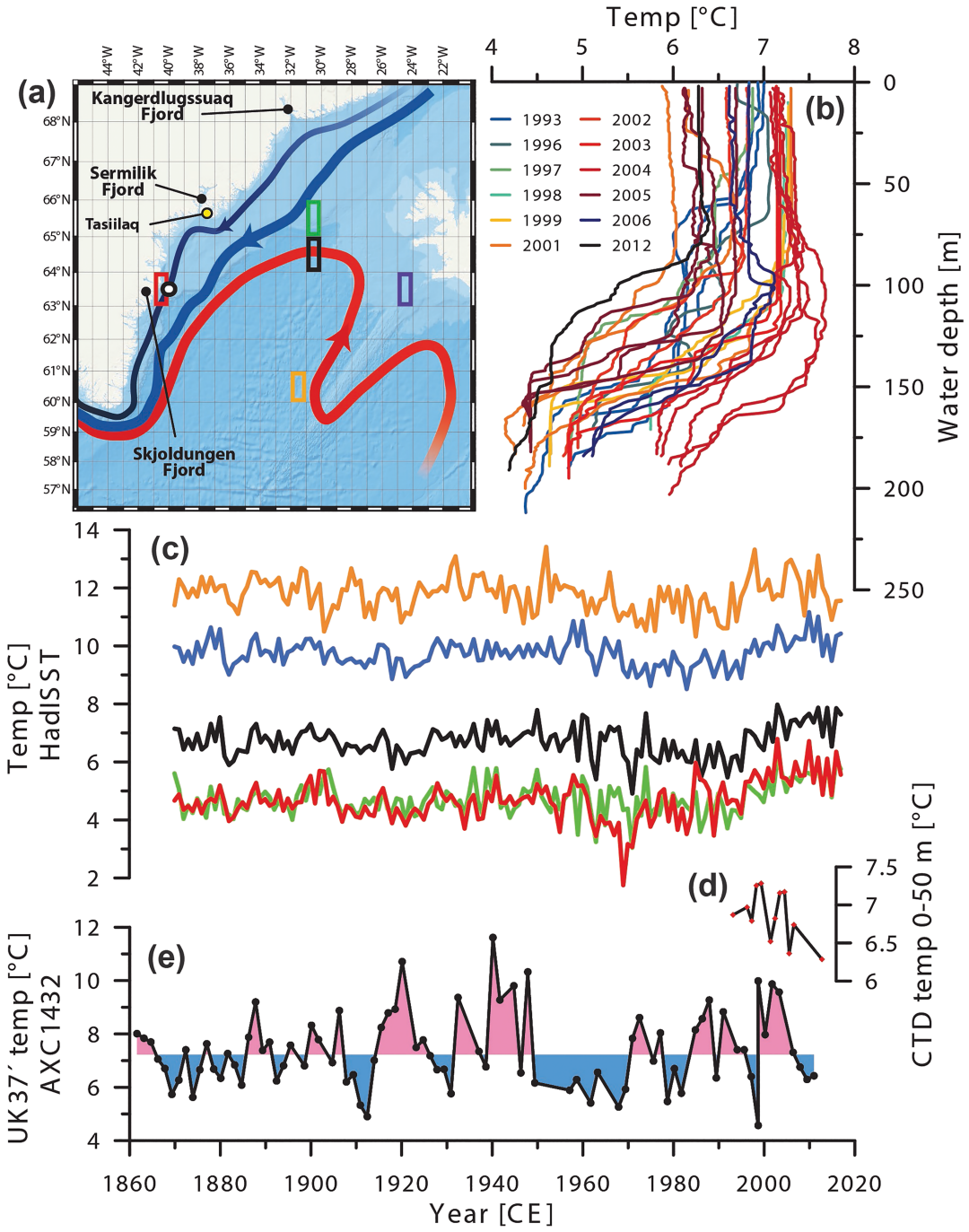

Figure 5. (a) Map showing the oceanography of SE-Greenland. Irminger Current (IC), East Greenland Current (EGC) and East Greenland coastal Current (EGCC); colored boxes indicate the location of the grid cells used in (c). White circle outside Nørre Skjoldungesund indicates the area of temperature profiles shown in (b). (b) Temperature profiles from outside Nørre Skjoldungesund from 1993 until 2012. All measurements were obtained in September (source: www.ICES.dk). (c) Average July–October HadISST temperature (Rayner et al., 2003), with the color code for each plot being related to the color of each box shown on the map in (a). (d) Average CTD temperature within the uppermost 50 m from (b). (e) BAYSPLINE AlkSST record from Nørre Skjoldungesund starting in 1860. Colors indicate variation from the average value 7.23°C.

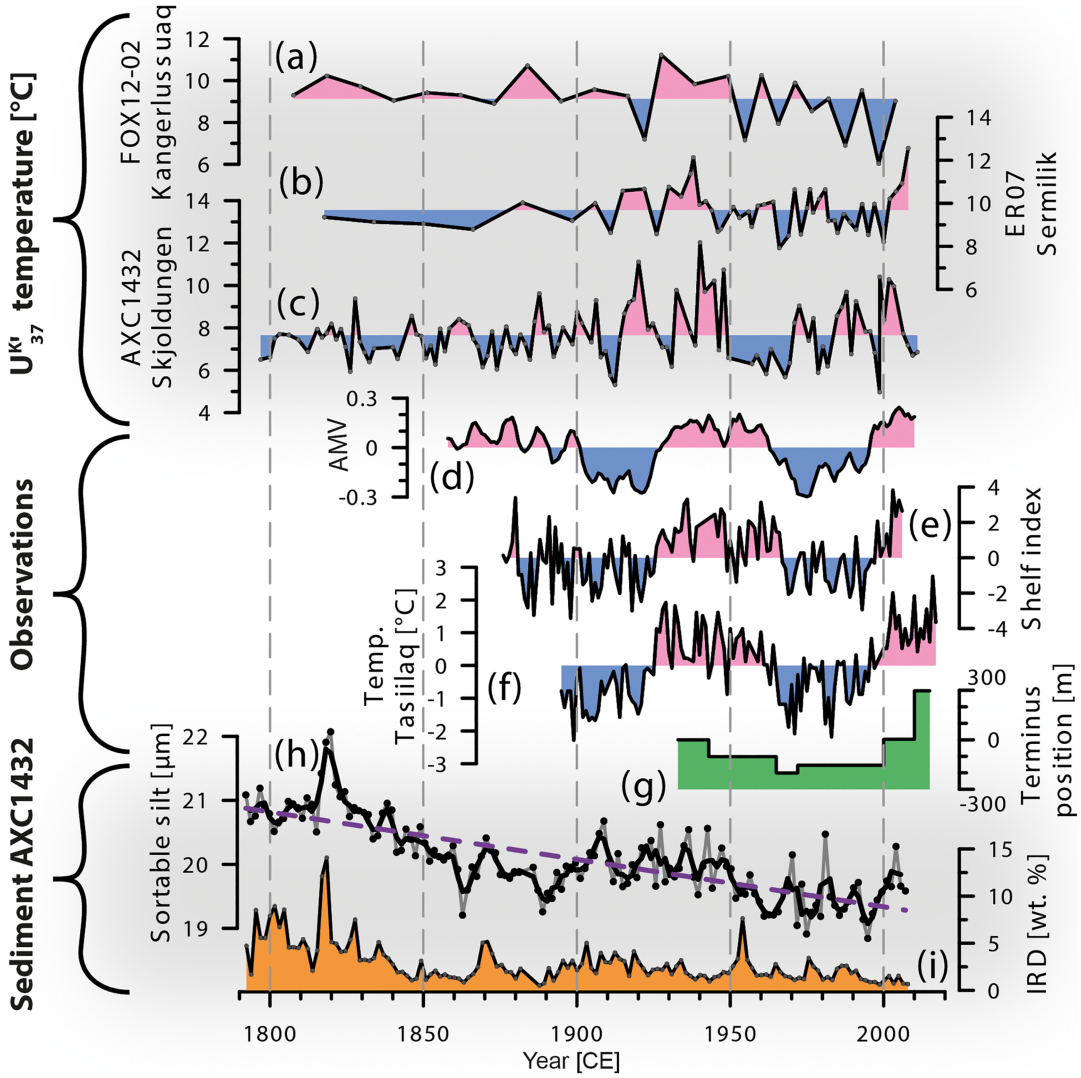

Figure 6. (a)–(c) AlkSST reconstructions from three fjords in SE-Greenland. (a) Kangerlussuaq Fjord, core FOX12-02 (Vermassen, Bjørk, et al., 2019), (b) Sermilik Fjord, core ER07 (Andresen et al., 2017), and (c) Nørre Skjoldungesund, core AXC1432 (this study, using the BAYSPLINE calibration). Colors indicate the variance from the individual average. (d) Atlantic Multidecadal Variability (AMV in *T*°C anomaly, Enfield et al., 2001), (e) Shelf Index (Andresen et al., 2013), (f) air temperature in Tasiilaq (Cappelen, 2018), (g) glacier terminus position of Thrym Glacier (negative values infer advance), (h) mean sortable silt of core AXC1432 applied with a 5-point running mean (black line) and linear trend line (purple dashed line), and (i) IRD signal from core AXC1432 in weight percentages of the combined sand fraction.

The influence of advected alkenones can also be further demonstrated by comparing the Nørre Skjoldungesund data with previous studies from Sermilik Fjord (Figure 6d; Andresen et al., 2017) and Kangerlussuaq Fjord (Figure 6e; Vermassen, Bjørk, et al., 2019), the latter being located 700 km north-east of Skjoldungen (Figure 5a). In all studies, the same alkenone-based method was used to reconstruct SSTs.

The average alkSST is 2.5°C and 1.9°C higher in the Sermilik Fjord record (9.7°C) and the Kangerlussuaq Fjord record (9.1°C), respectively, compared to the Nørre Skjoldungesund (7.2°C), indicating an even stronger influence of advected alkenones from upstream IC (Figures 5a and 5c). As the IC flows southwards, it gradually mixes with colder waters from the EGC (Sutherland et al.,

2013). Increased travel distance from the warmer regions of the IC and subsequent higher relative proportion of alkenones produced in the colder SE-Greenland shelf waters would account for lower mean temperatures in Nørre Skjoldungesund compared to Sermilik Fjord and Kangerlussuaq Fjord.

In summary, the alkSST record from Nørre Skjoldungesund reflects, in similarity with the alkSST records from Sermilik Fjord and Kangerlussuaq Fjord, qualitative variability of shelf waters. The temperature reconstruction undertaken on the fjord sediment is likely modulated by advection of detrital "warm"alkenones originating from upstream IC production area.

5.2. SST Variability on the SE-Greenland Shelf During the Last 220 Years

Comparison of the alkSST variability in Nørre Skjoldungesund with that of Sermilik Fjord (Andresen et al., 2017) reveals a significant correlation over the past 200 years ($R = 0.27$; $p < 0.005$), which suggests that both reconstructions feature common oceanographic variability over a wider region of the shelf (Figures 6e and 6f). The lower resolution alkSST reconstruction from Kangerlussuaq Fjord (Vermassen, Bjørk, et al., 2019) also shows broad resemblance after 1930 CE ($R = 0.33$; $p < 0.005$), but detailed comparison is hampered by the low temporal resolution of the record (Figure 6a).

A notable feature in all three alkSST records is a two-peaked maxima observed between 1915 and 1950 (Figures 6a–6c). A similar signal of higher temperature and a sharp cooling around 1950 was also reconstructed in the bottom water temperature in Disko Bay, West Greenland (Lloyd et al., 2011). This common feature reflects the oceanographic link between SE and West Greenland as the IC flows westward and impact the deeper West Greenland Current (WGC) in Disko Bay. The Atlantic Multidecadal Variability (AMV)—also called the Atlantic Multidecadal Oscillation (AMO)—is a oceanic mode expressing the decadal scale variability of SSTs in the North Atlantic Ocean (Schlesinger & Ramankutty, 1994, Sutton et al., 2018) (Figure 6c). Its basin wide warm and cold anomalies are also evident in air temperature instrumental observations from the SE-Greenland shelf (Figure 6d). However, although the alkSST records display multidecal variability in the 20th century, this pattern does not unequivocally resemble the AMV variability. Since the independently reconstructed and dated alkSST records from Skjoldungen, Sermilik, and Kangerlussuaq all document the onset of a multidecal warm period around 1915, thus about 15 years prior to the onset of AMV warming in 1930–1960, the AMV is likely not solely responsible for the warming pattern on the SE-Greenland shelf.

A previous sediment core study from SE-Greenland near Kangerlussuaq Fjord (Alonso-Garcia et al., 2013) documents a transition around 1910 CE from perennial sea ice cover along the coast of Greenland to seasonal sea ice cover and ice-free water during summer coinciding with the termination of the LIA in SE-Greenland (1890–1910 according to Bjørk et al., 2012). Reconstructions of sea ice flux from the Arctic Ocean via Fram Strait also document a marked transition approximately around 1910 to overall lower sea ice occurrence in the 20th century (Macias Fauria et al., 2010; Schmith & Hansen, 2003). This suggests that the decadal long SST maximum, commencing 1915, could in part be due to ice-free waters during summer on the SE-Greenland shelf.

The decrease in alkSST records from Skjoldungen, Sermilik, and Kangerlussuaq after c. 1950 occurred at a time when AMV evolved from a positive to a negative state. Likewise, it may be suggested that the decrease in SST on the SE-Greenland shelf after 1950 is linked with the concurrent higher sea ice occurrence in the EGC (Macias Fauria et al., 2010; Schmith & Hansen, 2003) and/or colder and less saline IC waters.

To explore the combined influence from changes in the IC and the EGC in the 20th century, Andresen et al. (2013) constructed the Shelf Index by combining a record of averaged SST from south of Iceland (20−30°W, 60−63°N), representing the IC variability, and the Storis index, which accounts for the southward flux of sea ice via the Fram Strait (Schmith & Hansen, 2003), thus reflecting the EGC variability (Figure 6e). A statistically significant correlation was found between Shelf Index and the alkSSTs of the shelf waters recorded in Sermilik Fjord sediments (Andresen et al., 2013). This supports the argument that the sea ice variability influences the SSTs on the SE-Greenland shelf including outside Nørre Skjoldungesund.

The cold decades after 1950 coincide with the Great Salinity Anomaly in the late 1960s to early 1970s, caused by the long-term decrease of the North Atlantic Oscillation index favoring the export of

freshwater and ice through Fram Strait into the EGC (Dickson et al., 1996). Within 2 or 3 years, the associated salinity anomaly reached the Labrador Sea causing a reduction of the convection and subsequent weakening of the Atlantic Meridional Overturning Circulation (AMOC). This mechanism explains the low temperature on the SE-Greenland shelf and the positive AMV during this time period (Ionita et al., 2016, Figure 6d).

While temperatures remain relatively low outside Sermilik and Kangerlussuaq Fjords, with a minor increase in the 1970s, the temperature record from Skjoldungen displays higher and rising temperature already in the 1970s and 1980s indicative of an early influence of the warm IC waters in this southernmost site, as the AMOC gradually resumes (Ionita et al., 2016). Sustained cold conditions at the northernmost site in Kangerlussuaq Fjord likely reflect the limit of influence of IC waters. The proxy record of bottom water temperature in Disko Bay also shows a marked warming starting in the 1970s (Lloyd et al., 2011) consistently reflecting the influence of IC propagating in the WGC.

The prominent warming observed in instrumental records after 2000 CE is evident in both the Skjoldungen and Sermilik records, possibly due to a weaker EGC than in the 1980s and a more north-south orientation and westwards location of the SPG in a weak mode allowing warmer and more saline waters of the IC to reach the Greenland shelf (Hátún et al., 2005).

Displayed in the alkSST record from Skjoldungen as well as in the CTD measurements off, Skjoldungen (Figure 5d) is a return to lower temperatures post 2006, pointing out the exceptional high temperatures around 2000.

5.3. Current Strength in the Fjord Water Column

Since the termination of the LIA, which ended between 1890 and 1910 in SE-Greenland (Bjørk et al., 2012), episodes of increased SS^{-} have occurred concurrently with episodes of increased SST on the shelf. Specifically, applying a 5-point running mean to the SS^{-} (Figure 6h, black line) reveals high values of SSTs and SS^{-} in the first half of the 20th century decreasing to lowest values in the 1970s, followed by three intervals with slightly higher values of SS^{-} and SSTs. A Pearson correlation between the alkSST record and the SS^{-} shows a very weak correlation ($R = -0.08$, $p > 0.05$) during the last 220 years, but a significant correlation ($R = 0.24$, $p < 0.05$) after AD 1915 (see Figure S2). A link between increasing SST and SS^{-} after 1915 may be explained by increased melting at the Thrym Glacier margin in response to increased air and/or ocean temperature resulting in enhanced meltwater plume dynamics and fjord circulation. Specifically, a further transport of the coarser silt fraction and more turbulence in the plume would cause an increase in flocculation that would modulate SS^{-} (Curran et al., 2004; Syvitski et al., 1996; Syvitski & Hutton, 1996).

Interestingly, the SS^{-} record from Nørre Skjoldungesund displays a long-term decreasing trend over the past 230 years (Figure 6h), very similar to a record reported by Thornalley et al. (2018) suggesting a common large-scale driver. The decreasing SS^{-} trend since the end of the LIA in sediments retrieved off Cape Hatteras in the western Atlantic Ocean (1,718-m water depth), was attributed to a weakening of the AMOC as a result of enhanced freshwater export from the Arctic including melting of Greenlandic glaciers (Thornalley et al., 2018). This positive buoyancy flux would have triggered anomalously low AMOC and reduced formation of Labrador Sea Water. Therefore, in addition to the meltwater dynamics, circulation in the Nørre Skjoldungesund Fjord may have also been partly controlled by the large-scale ocean circulation in the North Atlantic sector attributable to the dynamical features of the SPG. We point out that the 20th-century variations in SST and SS^{-} in our record are not entirely in phase and the exact processes linking these surface and deep records are unclear.

5.4. Iceberg Rafting Within Nørre Skjoldungesund

The IRD record from Nørre Skjoldungesund shows two longer periods of relatively high iceberg rafting, from the beginning of the record around 1796 to the 1830s with a major peak around 1829 and from 1890 to 1920 (Figure 6i). Shorter periods of increased IRD can be observed in the 1870s and in the 1950s, 1960s, 1970s, and 1980s. The periods with increased iceberg rafting are not coeval with a simultaneous increase in SSTs (Figure 6). Whereas the SST record shows a clear change in variability around 1900 CE, the IRD record remains relatively constant in this period. This is in contrast with studies of the larger marine terminating glaciers, for example, Jakobshavn Isbræ (Wangner et al., 2018) and Helheim Glacier (Andresen et al.,

2012), where increased IRD was related to observed glacier margin retreat and climate warming, suggesting a link between ocean forcing, iceberg production, and glacier retreat.

Changes in travel distance of the icebergs and the meltwater plume are not expected to have modulated the IRD variability significantly since the position of the glacier front has been relatively constant in the last 80 years. Skjoldmøen Glacier and possibly other small glaciers in the vicinity of the core site were at a more advanced position during the LIA, of which some may have calved of small icebergs, resulting in the higher IRD signal during the early 19th century. Low air and ocean temperatures during the LIA also could have led to an increase in sea ice formation and thereby rafting of debris transported by coastal ice. Short-term variations like in 1829 or 1952 can possibly be a result of stochastic distribution of IRD caused by turning or stuck icebergs. Altogether, while the higher IRD sedimentation in the early 19th century may be explained as a response to retreat of Skjoldmøen and other glaciers at the end of the LIA, the interannual variability in IRD in this relatively small fjord may have been modulated by multiple factors.

5.5. Steady Frontal Position of Thrym Glacier

Fluctuations of glacier termini since 1933 were highly variable in the SE-Greenland region. The front position of Bernstorffs Glacier, located about 30 km north of Thrym Glacier, was variable over a range of 6 km, whereas the front position of Rimfaxe/Guldfaxe, about 35 km south of Thrym Glacier, varied only by 150 m (Bjørk et al., 2012). Larger glaciers like Helheim Glacier or Jakobshavn Isbræ even retreated up to 5 and 20 km, respectively, within the same time period (Bjørk et al., 2012; Weidick & Bennike, 2007).

A plausible explanation for the relatively stable frontal position of Thrym Glacier (Figure 6g) could be the shallow bedrock underlying the glacier and possible shallow water depths in front of the glacier front (Figure 1). Similar to earlier findings in northwest and southeast Greenland, this would limit the ocean influence on the glacier front (Andresen, Kjeldsen, et al., 2014; Millan et al., 2018). The exact water depth at the glacier front is however hard to determine, as the recent version of Bedmachine v3 (Morlighem et al., 2017) provides little information about water depth and ice thickness at the glacier front due to the lack of input data. Modeled ice thickness in the lowermost 6 km of Thrym Glacier is estimated to 10 m over a prograding slope. Also, the model suggests a shallow uniform water depth of c. 50 m over a stretch of c. 4.5 km between the calving front and the measured multibeam data in Nørre Skjoldungesund, which record depths down to c. 350 m (Kjeldsen et al., 2017; Morlighem et al., 2017). Both estimates seem unlikely given the uniform water depth values over the large areas, though a shallow shoal close to the glacier cannot be ruled out. The apparent prograding slope underneath Thrym Glacier may cause the glacier to behave similar to a land-terminating glacier, thus decreasing the ice-ocean interface and making the glacier less sensitive to oceanographic variability inside the fjord (Millan et al., 2018; Morlighem et al., 2016).

Additionally, the inflow of warmer Atlantic water could be hampered by the 210-m shallow sill identified by Kjeldsen et al. (2017), which could explain the 1–1.5°C higher water temperatures below 200-m water depth at CTD14-07 compared to CTD14-06.

Moreover, the change in flow direction of Thrym Glacier as it passes through the valley systems may also play a role in its stability. As Thrym Glacier flows eastwards, it merges with the glacier from the north and the sidewalls of the fjord, both of which may act as pinning points. These combined factors may have concurred to keep the glacier margin position relatively stable despite ocean and climate fluctuations.

6. Conclusion

Reconstructed SSTs based on alkenones obtained from a sediment core in Nørre Skjoldungesund show high amplitude fluctuations between 5°C and 12°C, especially during the 20th century. Our SST data were compared to instrumental CTD data (ICES) and SST time series from several grid cells in the HadISST data set to trace the geographical source region of the deposited alkenones. The comparison with grid cells of the HadISST database shows that the alkSST record variability is mostly shaped by local shelf waters. However, the higher mean temperature indicates a significant influence of detrital alkenones advected

from IC upstream warmer waters. The influence from IC waters along the SE-Greenland coast is more strongly seen in other alkSST records from the more northern Sermilik Fjord and Kangerlussuaq Fjord. Comparison of these records indicates variable contributions of the EGC and the IC along the SE-Greenland shelf over the last century, with notable cold decades before 1915 and during the Great Salinity Anomaly in the 1960s. Warmer periods are observed between 1915 and 1950 and since the 1970s. Similar warm/cold features were also described downstream the WGC in Disko Bay in agreement with the circulation pattern of the region linking these different sites.

We found that the SST variability on the shelf waters outside Nørre Skjoldungesund may have influenced the glacier plume dynamics and/or current strength in the water column inside the fjord as evidenced by the SS^{-} sediment record. Specifically, SST changes over the 20th century may have caused an increase in the meltwater production of Thrym Glacier due to higher air temperatures and, with this, enhanced fjord circulation. The concurrent general decrease of SS^{-} and weakening in the AMOC suggest a role of the large-scale ocean circulation in the North Atlantic on the water dynamics in Nørre Skjoldungesund.

Our study shows that even though the meltwater production may have been influenced by climate, the glacier margin position and iceberg calving remained relatively constant in the 20th century. This may be due to the setting of the glacier with a limited ice-ocean interface and a 90° inflow angle acting as a pinning point in its current position. Our study illustrates that ocean heat may have a limited effect on some marine glaciers. We suggest that the specific setting (bedrock topography, flow angle) of individual glaciers as well as local temperature records needs to be considered in future model projections of climate change, ice sheet melt, and sea level rise to account for their contribution to the freshwater discharge in the North Atlantic.

Acknowledgments
This study is part of the project "Past and future dynamics of the Greenland Ice Sheet: What is the ocean hiding?" The authors thank the VILLUM Foundation for funding the project (grant no. 10100). This work was also supported by the National Natural Science Foundation of China (Grant Nos. 41776193 and 41876215). MAS thanks the Centre National de la Recherche Scientifique (CNRS) for salary support and the LEFE/INSU project NAIV for funding analysis. We thank the captain and crew of the SS ACTIV for their help during fieldwork. We also thank Pernille Stockmarr and Nanna Andreasen for helping during labwork, Laurence M. Dyke for fruitful discussions, and William Kenney for radioisotope measurements at UF. We also thank the two reviewers for valuable comments and suggestions on the manuscript. Data for Figures 3, 4, and 5 are available at https://doi.pangaea.de/10.1594/PANGAEA.908671.

References

Alonso-Garcia, M., Andrews, J. T., Belt, S. T., Cabedo-Sanz, P., Darby, D., & Jaeger, J. (2013). A comparison between multiproxy and historical data (ad 1990–1840) of drift ice conditions on the East Greenland Shelf (~66°N). *The Holocene*, *23*(12), 1672–1683. https://doi.org/10.1177/0959683613505343

Andresen, C. S., Kjeldsen, K. K., Harden, B., Nørgaard-Pedersen, N., & Kjær, K. H. (2014). Outlet glacier dynamics and bathymetry at Upernavik Isstrøm and Upernavik Isfjord, North-West Greenland. *Geological Survey of Denmark and Greenland Bulletin*, *31*(31), 79–82.

Andresen, C. S., Kokfelt, U., Sicre, M.-A., Knudsen, M. F., Dyke, L. M., Klein, V., et al. (2017). Exceptional 20th century glaciological regime of a major SE Greenland outlet glacier. *Scientific Reports*, *7*(1), 13626. https://doi.org/10.1038/s41598-017-13246-x

Andresen, C. S., McCarthy, D. J., Valdemar Dylmer, C., Seidenkrantz, M.-S., Kuijpers, A., & Lloyd, J. M. (2011). Interaction between subsurface ocean waters and calving of the JakobshavnIsbrae during the late Holocene. *The Holocene*, *21*(2), 211–224. https://doi.org/10.1177/0959683610378877

Andresen, C. S., Schmidt, S., Seidenkrantz, M.-S., Straneo, F., Grycel, A., Hass, C. H., et al. (2014). A 100-year record of changes in water renewal rate in Sermilik fjord and its influence on calving of Helheim Glacier, southeast Greenland. *Continental Shelf Research*, *85*, 21–29. https://doi.org/10.1016/j.csr.2014.05.017

Andresen, C. S., Sicre, M.-A., Straneo, F., Sutherland, D. A., Schmith, T., Hvid Ribergaard, M., et al. (2013). A 100-year long record of alkenone-derived SST changes by Southeast Greenland. *Continental Shelf Research*, *71*, 45–51. https://doi.org/10.1016/j.csr.2013.10.003

Andresen, C. S., Straneo, F., Ribergaard, M. H., Bjørk, A. A., Andersen, T. J., Kuijpers, A., et al. (2012). Rapid response of Helheim Glacier in Greenland to climate variability over the past century. *Nature Geoscience*, *5*(1), 37–41. https://doi.org/10.1038/ngeo1349

Andrews, J. T. (2000). Icebergs and iceberg rafted detritus (IRD) in the North Atlantic: Facts and assumptions. *Oceanography*, *13*(3), 100–108. https://doi.org/10.5670/oceanog.2000.19

Andrews, J. T., Smith, L. M., Preston, R., Cooper, T., & Jennings, A. E. (1997). Spatial and temporal patterns of iceberg rafting (IRD) along the East Greenland margin, ca. 68°N, over the last 14 cal.ka. *Journal of Quaternary Science*, *12*(1), 1–13.

Barrier, N., Cassou, C., Deshayes, J., & Treguier, A.-M. (2014). Response of North Atlantic Ocean Circulation to Atmospheric Weather Regimes. *Journal of Physical Oceanography*, *44*(1), 179–201. https://doi.org/10.1175/JPO-D-12-0217.1

Baty, F., Ritz, C., Charles, S., & Brutsche, M. (2015). A Toolbox for nonlinear regression in *R*: The package nlstools, *66*(5).

Bendle, J., Rosell-Melé, A., & Ziveri, P. (2005). Variability of unusual distributions of alkenones in the surface waters of the Nordic seas. *Paleoceanography*, *20*, PA2001. https://doi.org/10.1029/2004PA001025

Bianchi, G. G., & McCave, I. N. (1999). Holocene periodicity in North Atlantic climate and deep-ocean flow south of Iceland. *Nature*, *397*(6719), 515–517. https://doi.org/10.1038/17362

Bjørk, A. A., Kjær, K. H., Korsgaard, N. J., Khan, S. A., Kjeldsen, K. K., Andresen, C. S., et al. (2012). An aerial view of 80 years of climate-related glacier fluctuations in southeast Greenland. *Nature Geoscience*, *5*(6), 427–432. https://doi.org/10.1038/ngeo1481

Cappelen, J. (2018). DMI Report 18-04 Greenland—DMI Historical Climate Data Collection Colophon, 1–100.

Conte, M. H., Dickey, T. D., Weber, J. C., Johnson, R. J., & Knap, A. H. (2003). Transient physical forcing of pulsed export of bioreactive material to the deep Sargasso Sea. *Deep-Sea Research Part I: Oceanographic Research Papers*, *50*(10–11), 1157–1187. https://doi.org/10.1016/S0967-0637(03)00141-9

Conte, M. H., Sicre, M.-A., Rühlemann, C., Weber, J. C., Schulte, S., Schulz-Bull, D., & Blanz, T. (2006). Global temperature calibration of the alkenone unsaturation index (UK′37) in surface waters and comparison with surface sediments. *Geochemistry, Geophysics, Geosystems*, *7*, Q02005. https://doi.org/10.1029/2005GC001054

Curran, K. J., Hill, P. S., Milligan, T. G., Cowan, E. A., Syvitski, J. P. M., & Konings, S. M. (2004). Fine-grained sediment flocculation below the Hubbard Glacier meltwater plume, Disenchantment Bay, Alaska. *Marine Geology*, *203*(1–2), 83–94. https://doi.org/10.1016/S0025-3227(03)00327-X

Dickson, R., Lazier, J., Meincke, J., Rhines, P., & Swift, J. (1996). Long-term coordinated changes in the convective activity of the North Atlantic. *Progress in Oceanography*, *38*(3), 241–295. https://doi.org/10.1016/S0079-6611(97)00002-5

Dowdeswell, J. A. (1987). Processes of glacimarine sedimentation. *Progress in Physical Geography*, *11*, 52–90.

Dyke, L. M., Andresen, C. S., Seidenkrantz, M.-S., Hughes, A. L. C., Hiemstra, J. F., Murray, T., et al. (2017). Minimal Holocene retreat of large tidewater glaciers in Køge Bugt, southeast Greenland. *Scientific Reports*, *7*(1), 1–10. https://doi.org/10.1038/s41598-017-12018-x

Enfield, D. B., Mestas-Nuñez, A. M., & Trimble, P. J. (2001). The Atlantic multidecadal oscillation and its relation to rainfall and river flows in the continental U.S. *Geophysical Research Letters*, *28*(10), 2077–2080. https://doi.org/10.1029/2000GL012745

Filippova, A., Kienast, M., Frank, M., & Schneider, R. R. (2016). Alkenone paleothermometry in the North Atlantic: A review and synthesis of surface sediment data and calibrations. *Geochemistry, Geophysics, Geosystems*, *17*, 1370–1382. https://doi.org/10.1002/2015GC006106

Häkkinen, S., & Rhines, P. B. (2004). Decline of subpolar north Atlantic circulation during the 1990s. *Science*, *304*(5670), 555–559. https://doi.org/10.1126/science.1094917

Hátún, H., Sandø, A. B., Drange, H., Hansen, B., & Valdimarsson, H. (2005). Influence of the Atlantic subpolar gyre on the thermohaline circulation. *Science*, *309*(5742), 1841–1844. https://doi.org/10.1126/science.1114777

Holland, D. M., Thomas, R. H., de Young, B., Ribergaard, M. H., & Lyberth, B. (2008). Acceleration of Jakobshavn Isbræ triggered by warm subsurface ocean waters. *Nature Geoscience*, *1*(10), 659–664. https://doi.org/10.1038/ngeo316

Ionita, M., Scholz, P., Lohmann, G., Dima, M., & Prange, M. (2016). Linkages between atmospheric blocking, sea ice export through Fram Strait and the Atlantic Meridional Overturning Circulation. *Scientific Reports*, *6*(1), 32881. https://doi.org/10.1038/srep32881

Khan, S. A., Aschwanden, A., Bjørk, A. A., Wahr, J., Kjeldsen, K. K., & Kjær, K. H. (2015). Greenland ice sheet mass balance: A review. *Reports on Progress in Physics*, *78*(4), 046801. https://doi.org/10.1088/0034-4885/78/4/046801

Kjeldsen, K. K., Korsgaard, N. J., Bjørk, A. A., Khan, S. A., Box, J. E., Funder, S., et al. (2015). Spatial and temporal distribution of mass loss from the Greenland Ice Sheet since AD 1900. *Nature*, *528*(7582), 396–400. https://doi.org/10.1038/nature16183

Kjeldsen, K. K., Weinrebe, W., Bendtsen, J., Bjørk, A. A., & Kjær, K. H. (2017). Multibeam Bathymetry and CTD—Measurements in two fjord systems in Southeast Greenland. *Earth System Science Data Discussions*, *30*, 1–25. https://doi.org/10.5194/essd-2017-29

Knudsen, M. F., Jacobsen, B. H., Seidenkrantz, M. S., & Olsen, J. (2014). Evidence for external forcing of the Atlantic Multidecadal Oscillation since termination of the Little Ice Age. *Nature Communications*, *5*, 1–8. https://doi.org/10.1038/ncomms4323

Lloyd, J. M. (2006). Late Holocene environmental change in Disko Bugt, west Greenland: Interaction between climate, ocean circulation and Jakobshavn Isbrae. *Boreas*, *35*(1), 35–49. https://doi.org/10.1111/j.1502-3885.2006.tb01111.x

Lloyd, J. M. (2011). Interaction between subsurface ocean waters and calving ofthe Jakobshavn Isbrae during the late Holocene. *The Holocene*, *21*(2), 211–211. https://doi.org/10.1177/0959683610378877

Lloyd, J. M., Moros, M., Perner, K., Telford, R. J., Kuijpers, A., Jansen, E., & McCarthy, D. (2011). A 100 yr record of ocean temperature control on the stability of Jakobshavn Isbrae, West Greenland. *Geology*, *39*(9), 867–870. https://doi.org/10.1130/G32076.1

Macias Fauria, M., Grinsted, A., Helama, S., Moore, J., Timonen, M., Martma, T., et al. (2010). Unprecedented low twentieth century winter sea ice extent in the Western Nordic Seas since A.D. 1200. *Climate Dynamics*, *34*(6), 781–795. https://doi.org/10.1007/s00382-009-0610-z

McCave, I. N., & Andrews, J. T. (2019). Distinguishing current effects in sediments delivered to the ocean by ice. I. Principles, methods and examples. *Quaternary Science Reviews*, *212*, 92–107. https://doi.org/10.1016/j.quascirev.2019.03.031

McCave, I. N., Manighetti, B., & Robinson, S. G. (1995). Sortable silt and fine sediment size/composition slicing: Parameters for palaeocurrent speed and palaeoceanography. *Paleoceanography*, *10*, 593–610.

McCave, I. N., Thornalley, D. J. R., & Hall, I. R. (2017). Relation of sortable silt grain-size to deep-sea current speeds: Calibration of the 'Mud Current Meter'. *Deep-Sea Research Part I: Oceanographic Research Papers*, *127*(July), 1–12. https://doi.org/10.1016/j.dsr.2017.07.003

Meischner, D., & Rumohr, J. (1974). A light-weight, high-momentum gravity corer for subaqueous sediments. *Senckenbergiana Maritima*, *6*(1), 105–117.

Millan, R., Rignot, E., Mouginot, J., Wood, M., Bjørk, A. A., & Morlighem, M. (2018). Vulnerability of Southeast Greenland glaciers to warm Atlantic Water from Operation IceBridge and Ocean Melting Greenland data. *Geophysical Research Letters*, *45*, 2688–2696. https://doi.org/10.1002/2017GL076561

Morlighem, M., Rignot, E., & Willis, J. K. (2016). Improving Bed Topography Mapping of Greenland Glaciers Using NASA's Oceans Melting Greenland (OMG) Data. *Oceanography*, *29*(4), 62–71. https://doi.org/10.5670/oceanog.2016.99

Morlighem, M., Williams, C. N., Rignot, E., An, L., Arndt, J. E., Bamber, J. L., et al. (2017). BedMachine v3: Complete Bed Topography and Ocean Bathymetry Mapping of Greenland From Multibeam Echo Sounding Combined With Mass Conservation. *Geophysical Research Letters*, *44*, 11,051–11,061. https://doi.org/10.1002/2017GL074954

Motyka, R. J., Cassotto, R., Truffer, M., Kjeldsen, K. K., van As, D., Korsgaard, N. J., et al. (2017). Asynchronous behavior of outlet glaciers feeding Godthåbsfjord (Nuup Kangerlua) and the triggering of Narsap Sermia's retreat in SW Greenland. *Journal of Glaciology*, 1–21.

Motyka, R. J., Hunter, L., Echelmeyer, K. A., & Connor, C. (2003). Submarine melting at the terminus of a temperate tidewater glacier, LeConte Glacier, Alaska, U.S.A. *Annals of Glaciology*, *36*, 57–65. https://doi.org/10.3189/172756403781816374

Murray, T., Scharrer, K., James, T. D., Dye, S. R., Hanna, E., Booth, A. D., et al. (2010). Ocean regulation hypothesis for glacier dynamics in southeast Greenland and implications for ice sheet mass changes. *Journal of Geophysical Research*, *115*, F03026. https://doi.org/10.1029/2009JF001522

Myers, P. G., Kulan, N., & Ribergaard, M. H. (2007). Irminger Water variability in the West Greenland Current. *Geophysical Research Letters*, *34*, L17601. https://doi.org/10.1029/2007GL030419

Olsson, I. U. (1980). Content of 14C in Marine Mammals from Northern Europe. *Radiocarbon*, *22*(03), 662–675. https://doi.org/10.1017/S0033822200010031

Paasche, E. (2002). A review of the coccolithophorid *Emiliania huxleyi*. *Phycologia*, *40*(6), 503–529.

Prahl, F. G., Muehlhausen, L. A., & Zahnle, D. L. (1988). Further evaluation of long-chain alkenones as indicators of paleoceanographic conditions. *Geochimica et Cosmochimica Acta*, *52*(9), 2303–2310. https://doi.org/10.1016/0016-7037(88)90132-9

Prahl, F. G., & Wakeham, S. G. (1987). Calibration of unsaturation patterns in long-chain ketone compositions for palaeotemperature assessment. *Nature*, *330*(6146), 367–369. https://doi.org/10.1038/330367a0

Rayner, N. A., Parker, D. E., Horton, E. B., Folland, C. K., Alexander, L. V., Rowell, D. P., et al. (2003). Global analyses of sea surface temperature, sea ice, and night marine air temperature since the late nineteenth century. *Journal of Geophysical Research*, *108*(D14), 4407. https://doi.org/10.1029/2002JD002670

Reimer, P. J., Baillie, M. G. L., Bard, E., Bayliss, A., Beck, J. W., Blackwell, C., et al. (2013). Intcal13 and Marine13 Radiocarbon Age Calibration Curves 0–50,000 Years Cal Bp. *Radiocarbon*, *55*(4), 1869–1887. https://doi.org/10.2458/azu_js_rc.46.4183

Rühlemann, C., & Butzin, M. (2006). Alkenone temperature anomalies in the Brazil-Malvinas confluence area caused by lateral advection of suspended particulate material. *Geochemistry, Geophysics, Geosystems*, *7*, Q10015. https://doi.org/10.1029/2006GC001251

Schlesinger, M. E., & Ramankutty, N. (1994). An oscillation in the global climate system of period 65-70 years. *Nature*, *372*(6506), 508–509. https://doi.org/10.1038/372508a0

Schmith, T., & Hansen, C. (2003). Fram Strait Ice Export during the Nineteenth and Twentieth Centuries Reconstructed from a Multiyear Sea Ice Index from Southwestern Greenland. *Journal of Climate*, *16*, 2782–2791.

Schulz, M., & Mudelsee, M. (2002). REDFIT: estimating red-noise spectra directly from unevenly spaced paleoclimatic time series. *Computers & Geosciences*, *28*(3), 421–426. https://doi.org/10.1016/S0098-3004(01)00044-9

Sicre, M.-A., Bard, E., Ezat, U., & Rostek, F. (2002). Alkenone distributions in the North Atlantic and Nordic sea surface waters. *Geochemistry, Geophysics, Geosystems*, *3*(2), 1013. https://doi.org/10.1029/2001GC000159

Sicre, M.-A., Hall, I. R., Mignot, J., Khodri, M., Ezat, U., Truong, M. X., et al. (2011). Sea surface temperature variability in the subpolar Atlantic over the last two millennia. *Paleoceanography*, *26*, PA4218. https://doi.org/10.1029/2011PA002169

Sicre, M.-A., Weckström, K., Seidenkrantz, M. S., Kuijpers, A., Benetti, M., Masse, G., et al. (2014). Labrador current variability over the last 2000 years. *Earth and Planetary Science Letters*, *400*, 26–32. https://doi.org/10.1016/j.epsl.2014.05.016

Straneo, F., Curry, R. G., Sutherland, D. A., Hamilton, G. S., Cenedese, C., Våge, K., & Stearns, L. A. (2011). Impact of fjord dynamics and glacial runoff on the circulation near Helheim Glacier. *Nature Geoscience*, *4*(5), 322–327.

Straneo, F., & Heimbach, P. (2013). North Atlantic warming and the retreat of Greenland's outlet glaciers. *Nature*, *504*(7478), 36–43. https://doi.org/10.1038/nature12854

Straneo, F., Heimbach, P., Sergienko, O., Hamilton, G., Catania, G., Griffies, S., et al. (2013). Challenges to understanding the dynamic response of Greenland's marine terminating glaciers to oceanic and atmospheric forcing. *Bulletin of the American Meteorological Society*, *94*(8), 1131–1144. https://doi.org/10.1175/BAMS-D-12-00100.1

Straneo, F., Sutherland, D. A., Holland, D., Gladish, C., Hamilton, G. S., Johnson, H. L., et al. (2012). Characteristics of ocean waters reaching greenland's glaciers. *Annals of Glaciology*, *53*(60), 202–210. https://doi.org/10.3189/2012AoG60A059

Sutherland, D. A., & Pickart, R. S. (2008). The East Greenland Coastal Current: Structure, variability, and forcing. *Progress in Oceanography*, *78*(1), 58–77. https://doi.org/10.1016/j.pocean.2007.09.006

Sutherland, D. A., Straneo, F., Stenson, G. B., Davidson, F. J. M., Hammill, M. O., & Rosing-Asvid, A. (2013). Atlantic water variability on the SE Greenland continental shelf and its relationship to SST and bathymetry. *Journal of Geophysical Research: Oceans*, *118*, 847–855. https://doi.org/10.1029/2012JC008354

Sutton, R. T., McCarthy, G. D., Robson, J., Sinha, B., Archibald, A. T., & Gray, L. J. (2018). Atlanticmultidecadal variability and the U.K. acsis program. *Bulletin of the American Meteorological Society*, *99*(2), 415–425. https://doi.org/10.1175/BAMS-D-16-0266.1

Syvitski, J. P. M., Andrews, J. T., & Dowdeswell, J. A. (1996). Sediment deposition in an iceberg-dominated glacimarine environment, East Greenland: Basin fill implications. *Global and Planetary Change*, *12*(1–4), 251–270.

Syvitski, J. P. M., & Hutton, E. W. H. (1996). In situ characteristics of suspended particles as determined by the floc camera assembly FCA. *Journal of Sea Research*, *36*(1--2), 131–142.

Syvitski, J. P. M., & Shaw, J. (1995). Sedimentology and geomorphology of fjords. *Geomorphology and Sedimentology of Estuaries*, *53*, 113–178.

Ternois, Y., Sicre, M.-A., Boireau, A., Conte, M. H., & E, G. (1997). Evaluation of long-chain alkenones as paleo-temperature indicators in the Mediterranean Sea. *Deep Sea Research Part I: Oceanographic Research Papers*, *44*(2), 271–286. https://doi.org/10.1016/S0967-0637(97)89915-3

Thornalley, D. J. R., Oppo, D. W., Ortega, P., Robson, J. I., Brierley, C. M., Davis, R., et al. (2018). Anomalously weak Labrador Sea convection and Atlantic overturning during the past 150 years. *Nature*, *556*(7700), 227–230. https://doi.org/10.1038/s41586-018-0007-4

Tierney, J. E., & Tingley, M. P. (2018). BAYSPLINE: A new calibration for the alkenone paleothermometer. *Paleoceanography and Paleoclimatology*, *33*, 281–301. https://doi.org/10.1002/2017PA003201

Vermassen, F., Bjørk, A. A., Sicre, M.-A., Jaeger, J., Wangner, D. J., Kjeldsen, K. K., et al. (2019). Sea surface temperature reconstruction, ice-rafted debris measurements, and age model of core FOX12-02R. PANGAEA. https://doi.org/10.1594/PANGAEA.908232

Vermassen, F., Wangner, D. J., Dyke, L. M., Schmidt, S., Cordua, A. E., Kjær, K. H., et al. (2019). Evaluating ice-rafted debris as a proxy for glacier calving in Upernavik Isfjord, NW Greenland. *Journal of Quaternary Science*, *34*, 258–267. https://doi.org/10.1002/jqs.3095

Wangner, D. J., Jennings, A. E., Vermassen, F., Dyke, L. M., Hogan, K. A., Schmidt, S., et al. (2018). A 2000-year record of ocean influence on Jakobshavn Isbræ calving activity, based on marine sediment cores. *The Holocene*, *28*(11), 1731–1744. https://doi.org/10.1177/0959683618788701

Weidick, A., & Bennike, O. (2007). Quaternary glaciation history and glaciology of Jakobshavn Isbrae and the Disko Bugt region, West Greenland: A review. Geological Survey of Denmark and Greenland Bulletin.